International Journal of Engineering

Journal Homepage: www.ije.ir

Hybrid Analysis of Micropolar Ethylene-glycol Nanofluid on Stretching Surface Mounted Triangular, Rectangular and Chamfer Fins by FEM Strategy and Optimization with RSM Method

P. Pasha*[a], D. Domiri-Ganji[b]

[a] *Department of Mechanical Engineering, Mazandaran University of Science and Technology, Babol, Iran*
[b] *Department of Mechanical Engineering Noshirvani University of Technology, Babol, Iran*

PAPER INFO

Paper history:
Received 11 october 2020
Received in revised form 26 November 2021
Accepted 09 December 2021

Keywords:
Angular Velocity
Chamfer Fins
Finite Element Method
Nanofluid Effects

ABSTRACT

This paper analysis heat transfer and angular velocity of micropolar ethylene-glycol nanofluid over the triangular, rectangular and chamfer fins on the stretching sheet. The innovation of this paper is to investigate parameters of nanofluid flow passing from the different fins on the stretching surface. The finite Element Method is selected for solving governing equations. The nanofluid temperature in the space of fins is warm and equal to the surface temperature. The temperature value is 30 degrees. The maximum values of nanofluid temperature exist in the last fin of surfaces. By passing the nanofluid flow from the first fins of the surface, the temperature of flow comes from 25°C to 31°C and at the ends of the surface, the temperature is high value. The maximum of ethylene glycol angular velocity occurs at x=0.9 for chamfer and rectangular modes and the minimum of temperature occurs at x=0.8 for 3 different fins. The angular velocity for nanofluid on the triangular and chamfer modes is 6.5% bigger than other baffles.

***doi**: 10.5829/ije.2022.35.05b.01*

NOMENCLATURE

H	Distance the plates (m)	Nb	Brownian motion
C	Nanofluid concentration	T_c	Temperature of the cold wall (K)
K	Dimensionless temperature	ΔT	Temperature difference
x, y	Coordinates (m)	**Greek Symbols**	
u,v	Velocity components (m/s)	ρ	Density (kg/m^3)
θ	Dimensionless temperature	μ	Dynamic viscosity (kg/m. s)
ϑ	Kinematic viscosity (m^2/s)	β	Thermal expansion (1/K)
C_p	Specific heat at constant pressure (J/kg.k)	α	Thermal diffusivity (m^2/s)
k	Thermal conductivity (W/m.k)	ν	Kinematic viscosity (m^2/s)
P	Modified fluid pressure	$\emptyset$	Dimensionless concentration
g_y	Gravitational acceleration (m/s^2)	σ	Electrical conductivity (s/m)
Pr	Prandtl number (υ/α)	B_0	Magnetic field intensity
Nt	Thermo-phoretic parameter	σ_{nf}	Ferrofluid electric conductivity

1. INTRODUCTION

Thread stretching sheet with different fins at steady-state two-dimensional flow of a micropolar/classical ferro-fluid was investigated. A ferrofluid is a form of fluid that exists in which micro particles of iron, magnetite, or cobalt. Ferrofluids are made-up of magnetic iron pieces suspended in oil, commonly kerosene, with a surfactant

*Corresponding Author Email: pasha.pooya@yahoo.com (P. Pasha)

Please cite this article as: P. Pasha, D. Domiri-Ganji, Hybrid Analysis of Micropolar Ethylene-glycol Nanofluid on Stretching Surface Mounted Triangular, Rectangular and Chamfer Fins by FEM Strategy and Optimization with RSM Method, ***International Journal of Engineering, Transactions B: Applications*** Vol. 35, No. 05, (2022) 845-854

to prevent oleic acid. Ferrofluids and nanofluids are used in rotary seals in computer hard drives and other rotating shaft motors [1–9]. Ţălu et al. [10] investigated the fractal geometry of internal thread surfaces manufactured by cutting tap and rolling tap. The application of fractal geometry in internal threads surface characterization to disclose fault fine structures of the internal thread geometry caused by the manufacturing process is briefly presented in this work. Zheng and Dai [11] studied a new finite element method for computing structural stochastic responses of linear problems. The method decouples the stochastic response into a sequence of deterministic responses with random variable coefficients and gives a new expansion of stochastic response. Pasha et al. [12] investigated the analytical solution of non -Newtonian second–grade fluid flow by VIM and ADM methods on a stretching sheet. This study aimed at investigating the variation of heat transfer and velocity changes of the fluid flow along the vertical line on a surface drawn from both sides. Coggon [13] have reviewed electromagnetic and electrical modeling by the finite element method. The finite element approach is based on energy minimization in the solution of physical problems; in this case, electromagnetic energy is minimized. Numerical and analytical comparison of the stability and instability of angular motion of a bar drawn by a spring by AGM method reviewed by Pasha et al. [14]. Krishna et al. [15] have researched Hall and ion slip effects on unsteady MHD free convective rotating flow through a saturated porous medium. The present study has an immediate application in understanding the drag experienced at the heated and inclined surfaces. Tripathy et al. [16] investigated the chemical reaction effect on MHD free convective surface over a moving vertical plate. In this research, the nonlinear partial differential equations were transformed into a two-point limit value problem with the help of similarity and t variables. Sarkar and Sahoo [17] studied the unsteady MHD flow on a stretchable rotating disk with heat transfer. Turner and Weidman [18] investigated Homann stagnation-point flow impinging on a biaxially stretching surface. The normal impact of the axial flow of the Homann stagnation point on a surface running perpendicularly, planar, biaxial is investigated. Application of numerical methods in micropolar fluid flow and heat transfer in permeable reviewed by Pasha et al. [19]. Thread stretching sheet with different fins at steady-state two-dimensional flow of a micropolar/classical ferro fluid was investigated [20–32]. This paper analysis heat transfer and angular velocity of micropolar ethylene-glycol nanofluid over the triangular, rectangular, and chamfer fins on the stretching sheet and investigated the magnetism effect around the different fins. The innovation of this paper is to investigate parameters of nanofluid flow passing from different positions of the fins ({rectangular, triangular and chamfer fins}- {rectangular and chamfer fins}-{ rectangular and triangular fins}-{ triangular and chamfer fins}) on the stretching surface. The structure of this paper is a study on the differential equations of ethylene glycol nanofluid by finite element strategy. By this strategy, the magnetic parameter, velocity, and temperature of the nanofluid were studied in separate contours. The problem of grid study is shown in Figure 1 as flowsheet.

2. PROBLEM DEFINITION

On a stretching sheet with ten numbers of different fins in the $y > 0$ direction, a steady-state two-dimensional flow of a micropolar/classical ferrofluid was assumed as shown in Figure 2. In the geometry of this paper, we discussed the effect of using fins with different shapes on nanofluid heat transfer and nanofluid flow velocity. In the industry, heat transfer can be optimized and increased by using fans with different positions and at the same distance from each other. Triangular and rectangular and chamfer fins are used on the surfaces. Nanofluid flow is entered with 25 °C and angular velocity is entered from 1 direction and passes through the fins and surface. The surface temperature is 30°C and the surface have been stretched by velocity in the X direction ($UW(x) = ax$, $a>0$). The velocity in the x-direction is 2m/s and the velocity in the y-direction is 0.2m/s. In this paper, the effect of the magnetic force (B) on the surface is investigated. The finite element method is used for solving this case. The governing equation for ferrofluid was simulated as Follows. The physical properties of water and Ethylene- glycol nanofluid at 25 °C are summarized in Table 1.

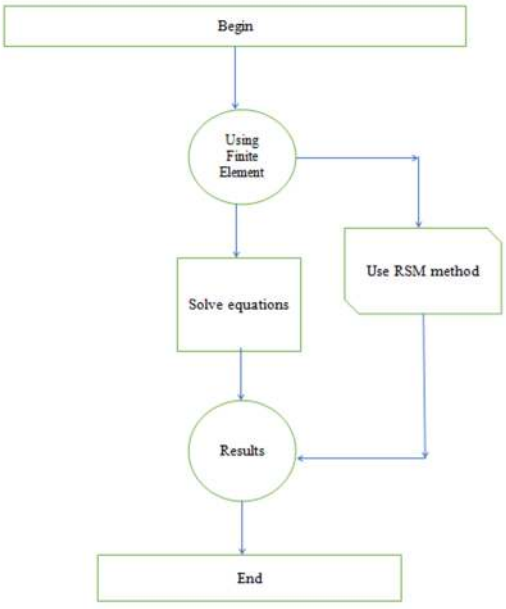

Figure 1. Grid study of the problem

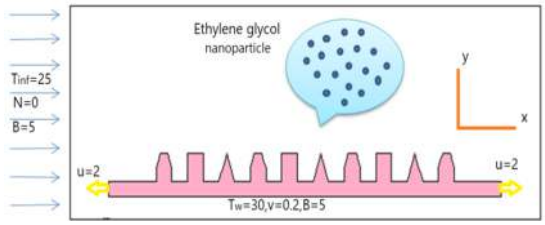

Figure 2. Schematic of different fins on the stretching sheet

TABLE 1. Properties of water and ethylene-glycol nanofluid at 25 °C [20]

	ρ (kg/m^3)	K (W/m.k)	C_p (J/kg.k)	σ
Ethylene glycol	1111	0.252	2415	57000
H_2O	997	0.613	4179	0.05

The finite element method is used to solve this case. In the below, the governing equation for ferrofluid is [27]:

$$\frac{d}{dt}(\rho_{nf}) = \nabla.(\rho_{nf} v) \quad (1)$$

$$\rho_{nf}\left(\frac{dv}{dt}\right) = -\nabla_p + (2\mu_{nf} + \aleph)\nabla(\nabla.v) - (\mu_{nf} + \aleph)\nabla.(\nabla.v) + \aleph(\nabla.N) + j.B + \rho_{nf} g \quad (2)$$

$$\rho_{nf} j\left(\frac{dN}{dt}\right) = (\varphi + \lambda + Y_{nf})\nabla.(\rho_{nf}.N) - Y_{nf}\nabla.(\nabla.N) + \aleph(\nabla.v) - 2\aleph N + \rho_{nf} I \quad (3)$$

where effective density, effective dynamic viscosity, and spin gradient viscosity are presented by Brinkman [21], Bourantas and Loukopoulos [22], respectively:

$$\rho_{nf} = (1-\varphi)\rho_f + \emptyset\rho_s \quad (4)$$

$$\mu_{nf} = \frac{\mu_f}{(1-\varphi)^{2.5}} \quad (5)$$

$$Y_{nf} = (\mu_{nf} + {}^{\aleph}/_{2})j \quad (6)$$

In addition, flow is incompressible in the absence of external forces. Therefore, equations will be difficult to solve.

$$\rho_{nf}\left(\frac{dv}{dt} + (v.\nabla)v\right) = (\mu_{nf} + \aleph)\nabla^2 v + \aleph(\nabla.N) + j.B \quad (7)$$

$$\rho_{nf} j\left(\frac{dN}{dt} + (N.\nabla)N\right) = Y_{nf}.\nabla^2 N + \aleph(\nabla.v) - 2\aleph N \quad (8)$$

and the body force proposed by hussanan et al. [23] is:

$$j.B = -\sigma_{nf} B_0^2 v \quad (9)$$

The ferrofluid electric conductivity represents [24]:

$$\sigma_{nf} = \left[1 + \frac{3(\sigma-1)\emptyset}{(\sigma+2)-(\sigma-1)\emptyset}\right]\sigma_f \quad (10)$$

and the governing equations would be:

$$\rho_{nf}\left(u\frac{du}{dx} + v\frac{du}{dy}\right) = (\mu_{nf} + \aleph)\frac{d^2u}{dy^2} + \aleph\frac{dN}{dy} - \sigma_{nf} B_0^2 u \quad (11)$$

$$\rho_{nf} j\left(u\frac{dN}{dx} + v\frac{dN}{dy}\right) = Y_{nf}\frac{d^2N}{dy^2} - \aleph\left(2N + \frac{du}{dy}\right) \quad (12)$$

The specific heat capacity and the effective thermal conductivities were defind by Mohyud-Din et al. [25].

$$C_{p,nf} = \frac{C_p)s+(1-\emptyset)(\rho C_p)f}{\rho_{nf}} \quad (13)$$

$$\frac{k_{nf}}{k_f} = \frac{k_s+2k_f-2\emptyset(k_f-k_s)}{k_s+2k_f+\emptyset(k_f-k_s)} \quad (14)$$

The energy equation represented as follows:

$$u\frac{dT}{dx} + v\frac{dT}{dy} = \frac{k_{nf}}{C_p)nf}\frac{d^2T}{dy^2} - \frac{dq_r}{dy} \quad (15)$$

It is stated as according to Roseland's approximation as follows:

$$u\frac{dT}{dx} + v\frac{dT}{dy} = \frac{1}{C_p)nf}\left(k_{nf} + \frac{16\sigma^* T_\infty^3}{3k^*}\right)\frac{d^2T}{dy^2} \quad (16)$$

The boundary conditions are:

$$u = au_w(x),\ v = v_w,\ at\ y = 0,\ u \leftrightarrow 0,\ y \to \infty \quad (17)$$

$$N = -\delta\frac{du}{dy}\ \ at\ \ y = 0,\ \ N \leftrightarrow 0,\ \ y \to \infty \quad (18)$$

$$T = T_w,\ at\ \ y = 0,\ \ T \leftrightarrow T_w,\ \ y \to \infty \quad (19)$$

In order to familiarize ourselves with these calculations, We have defined the velocity components in the x and y directions u and v, respectively. The suction and injection are represented by the positive and negative values of the surface mass transfer velocity, v_w. The angular velocity is denoted by N. μ is dynamic viscosity, and δ is a constant in the 0-1 range. When set to 0, the microelement is specified. If δ=1/2, the concentration of microelements was shown to be weak. Furthermore, when the turbulent boundary layer flow is required, δ=1. j represents microelement inertia per unit mass, where δ is spin gradient viscosity. To solve comfortably these nonlinear differential equations, we utilized similarity variables such as:

$$\eta = y\sqrt{\frac{a}{v_f}},\ u = axF'(\eta),\ v = -\sqrt{av_f}F(\eta),\ N = ax\sqrt{\frac{a}{v_f}}G(\eta,\ \theta(\eta) = \frac{T-T_\infty}{T_w-T_\infty}, \quad (20)$$

By substituting the variables in relations (20) in to the Equations (11), (12), (16), we have:

$$\left(\frac{1}{(1-\emptyset)^{2.5}} + k\right)F'''(\eta) + \left(1 - \emptyset + \emptyset\frac{\rho_s}{\rho_f}\right)F(\eta)F''(\eta) - \left(1 - \emptyset + \emptyset\frac{\rho_s}{\rho_f}\right)F'^2(\eta) - M\left(1 + \frac{3(\sigma-1)\emptyset}{\sigma+2-(\sigma-1)\emptyset}\right)F'(\eta) + kG'(\eta) = 0 \quad (21)$$

$$\left(\frac{1}{(1-\emptyset)^{2.5}}+\frac{k}{2}\right)G''(\eta)+\left(1-\emptyset+\emptyset\frac{\rho_s}{\rho_f}\right)F(\eta)G'(\eta)-\left(1-\emptyset+\emptyset\frac{\rho_s}{\rho_f}\right)F'(\eta)G(\eta)-k\left(2G(\eta)+F''(\eta)\right)=0 \quad (22)$$

$$\frac{1}{Pr}\left(\frac{k_s+2k_f-2\emptyset(k_f-k_s)}{k_s+2k_f+\emptyset(k_f-k_s)}+R\right)\theta''(\eta)+\left(1-\emptyset+\frac{C_p)s}{C_p)f}\right)F(\eta)\theta'(\eta)=0 \quad (23)$$

and here the new boundary conditions are:

$$F(\eta)=S, F'(\eta)=\alpha, G(\eta)=-\delta F''(\eta), \theta(\eta)=1, \quad at\ \eta=0 \quad (24)$$

$$F'(\eta)\leftrightarrow 0, G(\eta)\leftrightarrow 0, \theta(\eta)\to 0 \quad at\ \eta\to\infty \quad (25)$$

3. SIMULATION METHODOLOGY

3. 1. Finite Element Method (FEM) Finite Element Method is an important numerical method that one of the practical applications for this method is Flexpde software, That is solved the nonlinear partial differential equations and ordinary differential equations.The output of the results FlexPDE is also a 'problem-solving environment' that executes the full range of functions required to resolve partial differential equation systems. The finite element method is a numerical method for solving partial differential equations defined based on one or two spatial variables. In this method, to solve the problem, a large system is divided into smaller and simpler parts called finite elements. This spatial discretization requires defining the object or environment of the problem as a network, or mesh.

According to Figure 3, the largest grid of mesh is around the edges, because around the baffles the fluid properties such as temperature and velocity of nanofluid flow changed.

3. 2. Validation for Methods In this section, for validation, we compared our work with Jalili et al. [20]. The computational error in our work is very low compared to others. The maximum number of errors happened when η=1.5 and minimum number of errors happened when η=1. Figure 4 shows comparison of data presentations for present study and Jalili et al. [20]. The Comparison of velocity for present work and Jalili's work at K=10, δ=0.5, ϕ=0.03 are summarized in Table 2.

4. RESULTS AND DISCUSSION

Figure 5 shows the nanofluid velocity is low around the space of the surface and fins. The maximum nanofluid velocity is attached to the surface of fins. The value of the maximum velocity is 2 m/s. By increasing the

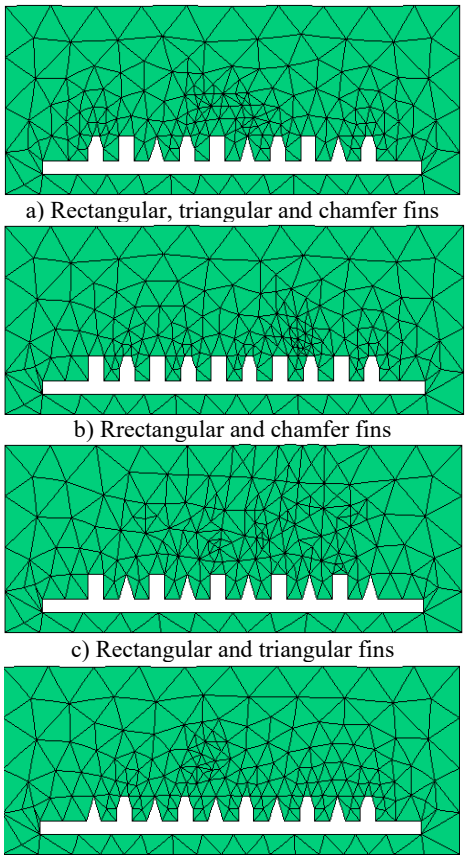

Figure 3. Comparison of mesh geometry for stretching surface

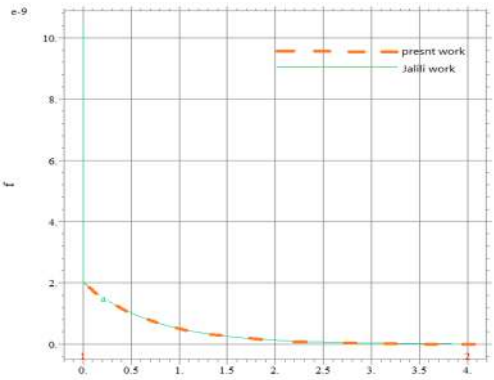

Figure 4. Comparison of velocity for present work and Jalili [20] at K=10, δ=0.5, ϕ =0.03

TABLE 2. Comparison of velocity for present work and Jalili work at K=10, δ=0.5, ϕ =0.03

	$\eta=0.0$	$\eta=1$	$\eta=1.5$	$\eta=2$	$\eta=2.5$	$\eta=4$
Present work	2	0.8	0.6	0.5	0.3	0
Jalili et al. [20]	2	0.8	0.6	0.5	0.3	0

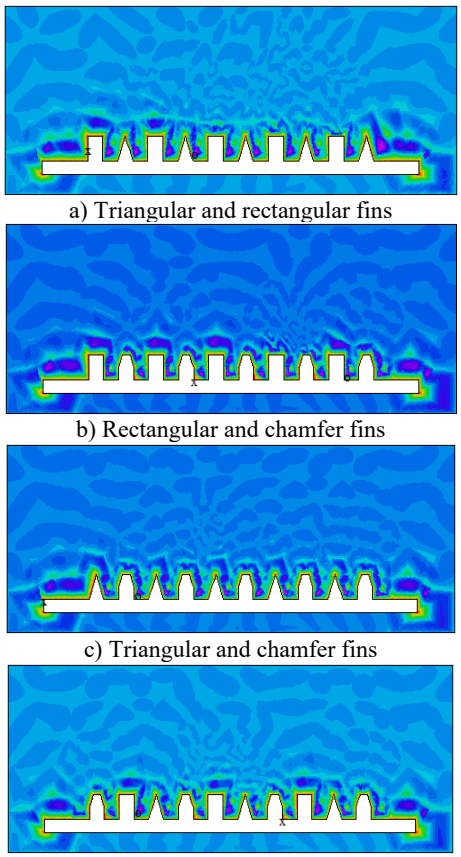

a) Triangular and rectangular fins

b) Rectangular and chamfer fins

c) Triangular and chamfer fins

d) Rectangular, triangular and chamfer fins

Figure 5. Comparison of velocity changes in the X direction in different fins for stretching surface

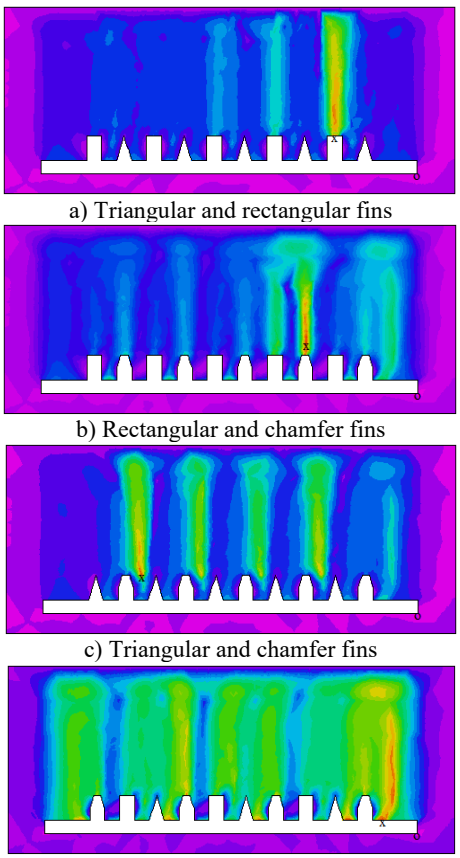

a) Triangular and rectangular fins

b) Rectangular and chamfer fins

c) Triangular and chamfer fins

d) Rectangular, triangular and chamfer fins

Figure 6. Comparison of angular velocity changes in different fins for stretching surface

distance of nanofluid from the surface, the velocity is reduced but by decreasing the distance from the surface, the velocity is increased. By comparing modes a-5 and b-5 we find that if we use a triangular blade instead of a chamber blade, we create a larger velocity gradient.

Figure 6 shows the angular velocity of nanofluid flow passing the stretching surface. On the surface, many fins exist, such as rectangular fins, triangular and chamfer fins. Under the surface, the angular velocity of nanofluid is very low but on the surface and near the fins, the angular velocity increases. In general, the angular velocities near the rectangular and chamfer fins (b-6) have an additional value than the triangular fins, because the surface of their side is larger than the triangular side. With an increase in variety of the fins (d-6) on the surface, the angular velocity of nanofluid has a maximum value.

Figure 7 shows the changes of nanofluid temperature passing the stretching surface. The nanofluid temperature in the space of fins is warm and equal to the surface temperature. The value of temperature is 30°C. The maximum values of nanofluid temperature exist in the last fin of surfaces. By passing the nanofluid flow from the first fins of the surface, the flow temperature increased from 25 to 31°C and at the ends of the surface, the temperature is high. Due to the different positions of the fin at the top of the page, we find that if we use a chamfer blade at the top of the page, we create a larger temperature gradient than other modes.

The vectors of angular velocity for nanofluid flow are shown in Figure 8. The most dispersion of velocity (N) is shown in Figure 8d. As in the middle of the surface near the third and eighth fins, the value of angular velocity is low and at the beginning and the end, the value of velocity is high.

Figure 9 shows the changes of nanofluid flow near the rectangular and triangular and chamfer fins in the chart. The lowest value of velocity in the x-direction of nanofluid flow is in the x=0 to x=0.1 with u=0.3m/s. the maximum velocity in the x-direction is 2m/s. The variations in velocity all over the different fins are very high.

In the state of triangular and chamfer fins (b-10) on the surface, the maximum angular velocity exists at x=0.2 near the first fins. The value of the velocity at x=0.2 is 400. In the position of different fins shapes next to each other (triangular and rectangular and chamfer), most changes of angular velocity are created in the x=0 to x=1.

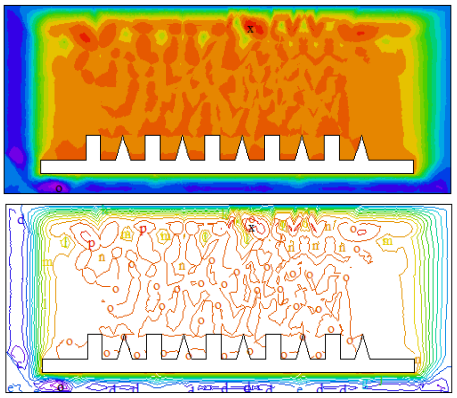

a) Triangular and rectangular fins

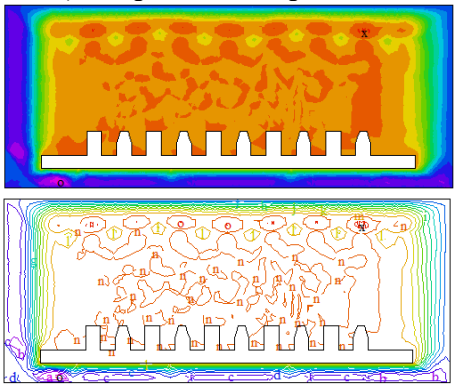

b) Rectangular and chamfer fins

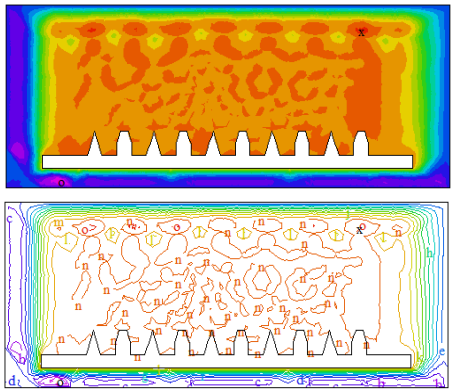

c) Triangular and chamfer fins

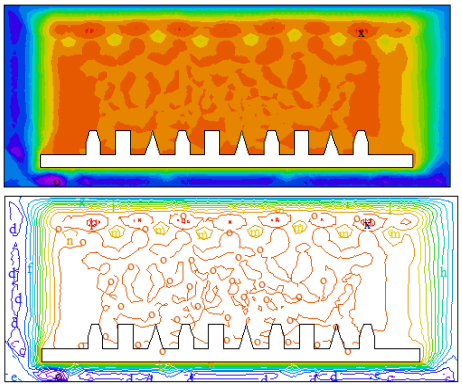

d) Rectangular, triangular and chamfer fins

Figure 7. Comparison of temperature profiles for threated stretching surface with different fins

In the same case, the velocity has a variation in the modes. In the x=0, the value of angular velocity is 30 and in x=0.4, the value of velocity is N=150.

Figure 11 shows the changes of nanofluid temperature passing the stretching surfaces. The value of temperature begins from 28 to 31°C all over the different fins. The temperature of nanofluid in the x=0.2 to x=0.8 have a constant value (T=30 °C) and no changes around the fins.

According to Table 3, the maximum ethylene glycol temperature occurs in the x=0.1 for three different fins, and the minimum temperature occurs in the x=0 for 3 different fins. The maximum nanofluid temperature is T=30.36°C and minimum temperature is T=28.13°C. The maximum temperature change exists around the 3 different (rectangular, triangular and chamfer) baffles, and the thermal boundary layer in this position is larger than in other cases. The nanofluid temperature on the 3 different fins is 4.5% bigger than chamfer and rectangular fins and 5.34% bigger than chamfer and triangular modes. Due to the different positions of the fin at the top of the page, we find that if we use a chamfer blade at the top of the page, we create a larger temperature gradient than other modes.

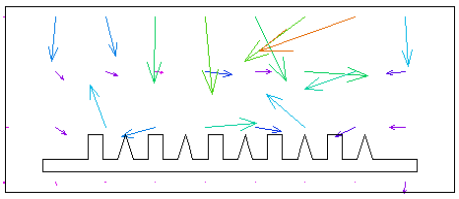

a) Triangular and rectangular fins

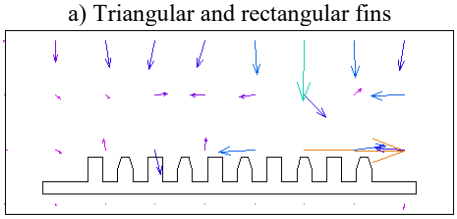

b) Rectangular and chamfer fins

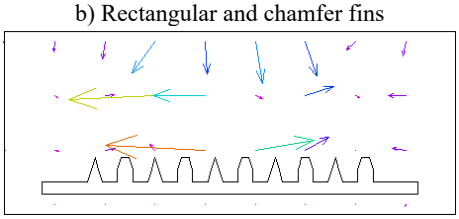

c) Triangular and chamfer fins

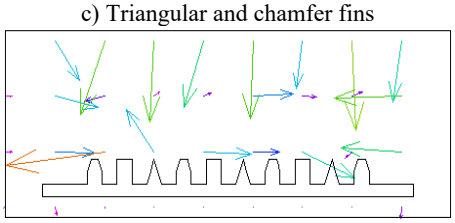

d) Rectangular, triangular and chamfer fins

Figure 8. Comparison of vector grid temperature changes in different fins for stretching surface

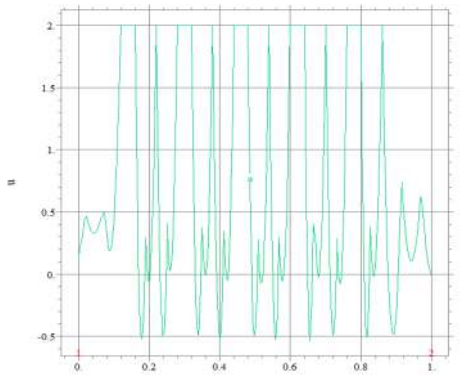

a) Triangular and rectangular fins

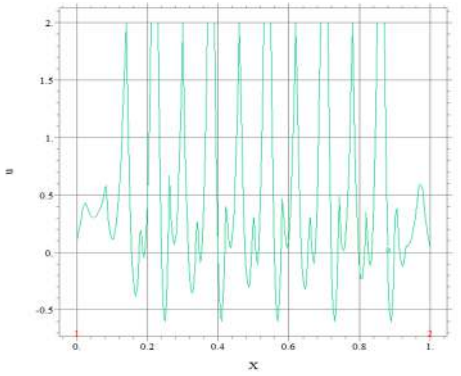

b) Triangular and chamfer fins

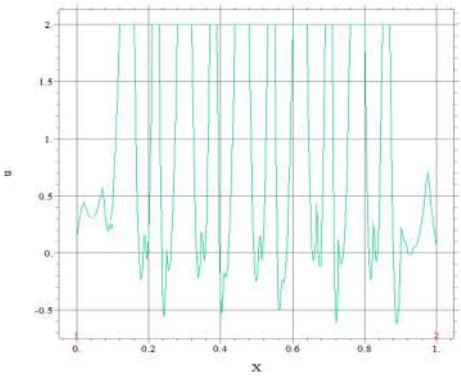

c) Rectangular and chamfer fins

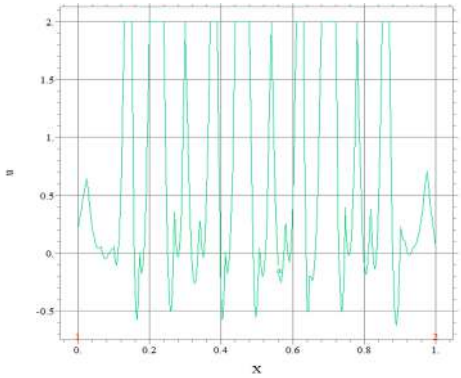

d) Rectangular, triangular and chamfer fins

Figure 9. Comparison of velocity (u) changes in in rectangular and triangular fins for threated stretching surface

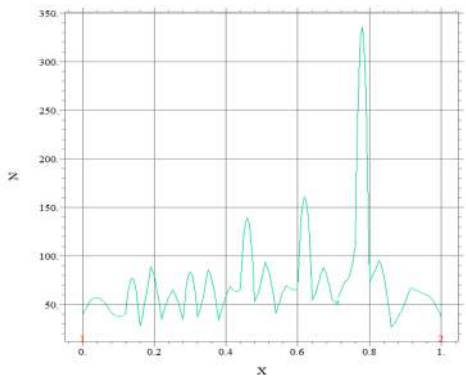

a) Triangular and rectangular fins

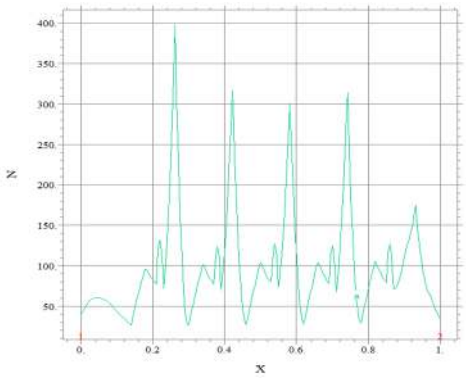

b) Triangular and chamfer fins

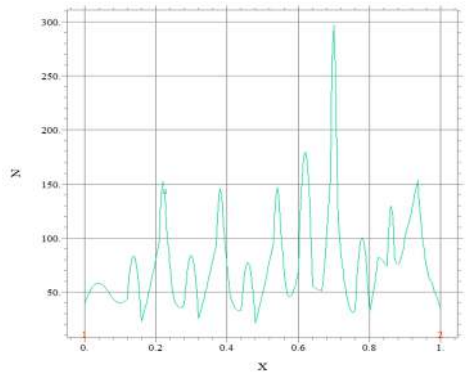

c) Rectangular and chamfer fins

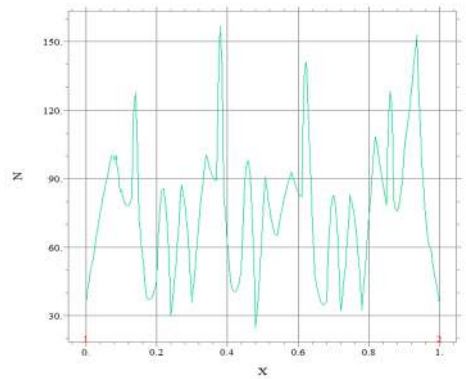

d) Rectangular, triangular and chamfer fins

Figure 10. Comparison of angular velocity changes in in rectangular and triangular fins for threated stretching surface

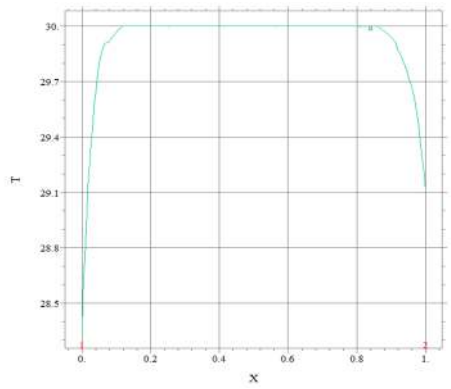

a) Triangular and rectangular fins

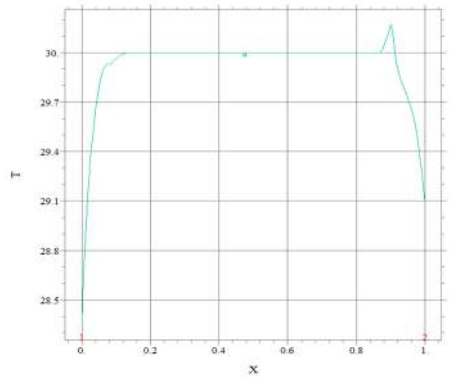

b) Triangular and chamfer fins

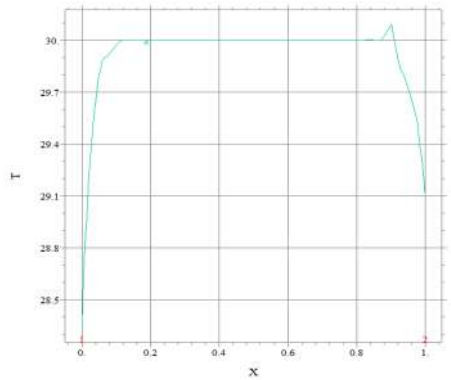

c) Rectangular and chamfer fins

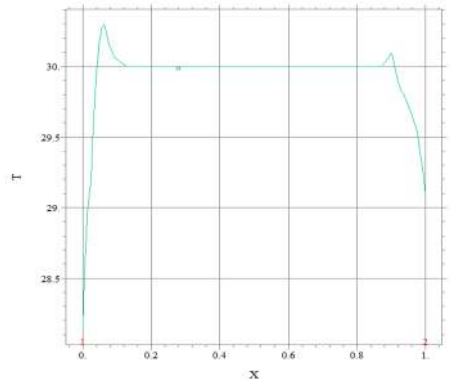

d) Rectangular, triangular and chamfer fins

Figure 11. Comparison of temperature changes in in rectangular and triangular fins for threated stretching surface

TABLE 3. Numerical comparison of temperature between different modes of fins

η	$T_{3\text{ different fins}}$	$T_{\text{chamfer and rectangular}}$	$T_{\text{chamfer and triangular}}$	$T_{\text{rectangular and triangular}}$
0	28.13	28.33	28.34	28.33
0.1	30.36	29.94	29.96	29.89
0.2	30.00	30.00	29.99	29.97
0.5	30.00	30.00	29.99	29.97
0.8	29.99	30.00	30.00	29.99
0.9	30.09	30.08	30.34	29.83
1	29.09	29.09	29.09	29.11

According to Table 4, the maximum of ethylene glycol velocity occurs in the x=0.3with T=399.98 for chamfer and triangular modes and the minimum of temperature occurs in the x=0.8 with T=33.34 °C for 3 different fins. The angular velocity for nanofluid on the triangular and chamfer modes is 34.5% bigger than 3different baffles and 58.54% bigger than chamfer and rectangular baffles. The most boundary condition for angular velocity shown around the initial baffles of the stretching sheet.

TABLE 4. Numerical comparison of angular velocity between different modes of fins

η	$N_{3\text{ different fins}}$	$N_{\text{chamfer and rectangular}}$	$N_{\text{chamfer and triangular}}$	$N_{\text{rectangular and triangular}}$
0	37.85	49.97	49.95	49.95
0.1	100.99	48.87	48.01	47.76
0.2	43.33	45.25	399.98	46.06
0.5	57.87	47.89	69.33	76.55
0.8	33.34	46.76	70.90	77.89
0.9	89.08	120.43	89.05	55.48
1	34.04	47.56	48.02	48.76

5. CONCLUSION

In this paper, variation of temperature and velocity in the x-direction and the angular velocity of the nanofluid flow through triangular and rectangular fins are investigated in the existence of a uniform magnetic field. The innovation of this paper is to investigate parameters of nanofluid flow passing from the different fins on the stretching surface. The finite element method is selected for solving governing equations.

- The effect of velocity changes in the x-direction around the baffles has more value than the surrounding space. The amount of flow velocity is reduced by increasing the distance from the surface in the y-

direction. General, the angular velocities near the rectangular fins and chamfer fins have an additional value than the triangular fins, because the surface of their side is larger than the triangular side. With the increasing, variation of the fins on the surface, the angular velocity of nanofluid has a maximum value.

- The temperature of nanofluid in the space of fins is warm and equal to the temperature of a surface. The value of temperature is 30°C. The maximum values of nanofluid temperature exist in the last fin of surfaces. By passing the nanofluid flow from the first fins of the surface, the temperature of flow comes from 25 to 31°C and at the ends of the surface, the temperature is high.
- The lowest value of velocity in the x -direction of nanofluid flow is in the x=0 to x=0.1 by u=0.3m/s. the maximum velocity in the x direction is 2m/s. changes in velocity all over the different fins are very high.
- In the state of triangular and chamfer fins together on the surface, the maximum angular velocity exists at x=0.2 near the first fins. The value of velocity at x=0.2 is 400. In the position of different fins shapes next to each other (triangular and rectangular and chamfer), most changes of angular velocity are created in the x=0 to x=1. In the same case, the velocity has a variation the modes. In the x=0, the value of angular velocity is 30 and in x=0.4, the value of velocity is N=150. The angular velocity for nanofluid on the triangular and chamfer modes is 6.5% more than other baffles.
- The value of temperature begins from 28 to 31°C in all over the different fins. The temperature of nanofluid in the x=0.2 to x=0.8 have a constant value (T=30°C) and no changes around the fins.

6. REFERENCES

1. Atashafrooz, M., Sajjadi, H., Amiri Delouei, A., Yang, T.-F., and Yan, W.-M. "Three-dimensional analysis of entropy generation for forced convection over an inclined step with presence of solid nanoparticles and magnetic force." ***Numerical Heat Transfer, Part A: Applications***, Vol. 80, No. 6, (2021), 318–335. https://doi.org/10.1080/10407782.2021.1944579
2. Atashafrooz, M. "Influence of radiative heat transfer on the thermal characteristics of nanofluid flow over an inclined step in the presence of an axial magnetic field." ***Journal of Thermal Analysis and Calorimetry***, Vol. 139, No. 5, (2020), 3345–3360. https://doi.org/10.1007/s10973-019-08672-0
3. Atashafrooz, M., Sajjadi, H., and Delouei, A. A. "Interacting influences of Lorentz force and bleeding on the hydrothermal behaviors of nanofluid flow in a trapezoidal recess with the second law of thermodynamics analysis." ***International Communications in Heat and Mass Transfer***, Vol. 110, (2020), 104411. https://doi.org/10.1016/j.icheatmasstransfer.2019.104411
4. Atashafrooz, M. "The effects of buoyancy force on mixed convection heat transfer of MHD nanofluid flow and entropy generation in an inclined duct with separation considering Brownian motion effects." ***Journal of Thermal Analysis and Calorimetry***, Vol. 138, No. 5, (2019), 3109–3126. https://doi.org/10.1007/s10973-019-08363-w
5. Atashafrooz, M., Sheikholeslami, M., Sajjadi, H., and Amiri Delouei, A. "Interaction effects of an inclined magnetic field and nanofluid on forced convection heat transfer and flow irreversibility in a duct with an abrupt contraction." ***Journal of Magnetism and Magnetic Materials***, Vol. 478, (2019), 216–226. https://doi.org/10.1016/j.jmmm.2019.01.111
6. Sheikholeslami, M., Sajjadi, H., Amiri Delouei, A., Atashafrooz, M., and Li, Z. "Magnetic force and radiation influences on nanofluid transportation through a permeable media considering Al2O3 nanoparticles." ***Journal of Thermal Analysis and Calorimetry***, Vol. 136, No. 6, (2019), 2477–2485. https://doi.org/10.1007/s10973-018-7901-8
7. Atashafrooz, M. "Effects of Ag-water nanofluid on hydrodynamics and thermal behaviors of three-dimensional separated step flow." ***Alexandria Engineering Journal***, Vol. 57, No. 4, (2018), 4277–4285. https://doi.org/10.1016/j.aej.2017.07.016
8. Yamini, O. A., Kavianpour, M. R., and Movahedi, A. "Performance of Hydrodynamics Flow on Flip Buckets Spillway for Flood Control in Large Dam Reservoirs." ***Journal of Human, Earth, and Future***, Vol. 1, No. 1, (2020), 39–47. https://doi.org/10.28991/HEF-2020-01-01-05
9. Aminoroayaie Yamini, O., Mousavi, S. H., Kavianpour, M. R., and Safari Ghaleh, R. "Hydrodynamic Performance and Cavitation Analysis in Bottom Outlets of Dam Using CFD Modelling." ***Advances in Civil Engineering***, Vol. 2021, , (2021), 1–14. https://doi.org/10.1155/2021/5529792
10. Ţălu, Ş., Kulesza, S., Bramowicz, M., Sağlam, H., and Kus, R. "Fractal geometry of internal thread surfaces manufactured by cutting tap and rolling tap." ***Manufacturing Letters***, Vol. 23, (2020), 34–38. https://doi.org/10.1016/j.mfglet.2019.12.001
11. Zheng, Z., and Dai, H. "Structural stochastic responses determination via a sample-based stochastic finite element method." ***Computer Methods in Applied Mechanics and Engineering***, Vol. 381, (2021), 113824. https://doi.org/10.1016/j.cma.2021.113824
12. Pasha, P., Nabi, H., Asadi, Z., and Domairry Ganji, D. "Analytical solution of non -Newtonian second –grade fluid flow by VIM and ADM methods on a stretching sheet." In 1st Conference on Electrical, Mechanical and Engineering Sciences, (2021), 1–17. Retrieved from https://civilica.com/doc/1170934
13. Coggon, J. H. "Electromagnetic and electrical modeling by the finite element method." ***Geophysics***, Vol. 36, No. 1, (1971), 132–155. https://doi.org/10.1190/1.1440151
14. Pasha, P., Nabi, H., and Domairry Ganji, D. "Numerical and analytical comparison of the stability and instability of angular motion of a bar drawn by a spring by AGM method." In 5th National Conference on Application of Novel Technologies in Engineering Sciences,Torbat Heydarieh (2021), 1–9. Retrieved from https://civilica.com/doc/1202840
15. Veera Krishna, M., Ameer Ahamad, N., and Chamkha, A. J. "Hall and ion slip effects on unsteady MHD free convective rotating flow through a saturated porous medium over an exponential accelerated plate." ***Alexandria Engineering Journal***, Vol. 59, No. 2, (2020), 565–577. https://doi.org/10.1016/j.aej.2020.01.043
16. Tripathy, R. S., Dash, G. C., Mishra, S. R., and Baag, S. "Chemical reaction effect on MHD free convective surface over a moving vertical plate through porous medium." ***Alexandria Engineering Journal***, Vol. 54, No. 3, (2015), 673–679. https://doi.org/10.1016/j.aej.2015.04.012
17. Sarkar, G. M., and Sahoo, B. "On dual solutions of the unsteady MHD flow on a stretchable rotating disk with heat transfer and a linear temporal stability analysis." ***European Journal of Mechanics - B/Fluids***, Vol. 85, (2021), 149–157. https://doi.org/10.1016/j.euromechflu.2020.09.010
18. Turner, M. R., and Weidman, P. "Homann stagnation-point flow

impinging on a biaxially stretching surface." ***European Journal of Mechanics - B/Fluids***, Vol. 86, (2021), 49–56. https://doi.org/10.1016/j.euromechflu.2020.11.010

19. Pasha, P., Mirzaei, S., and Zarinfar, M. "Application of numerical methods in micropolar fluid flow and heat transfer in permeable plates." ***Alexandria Engineering Journal***, Vol. 61, No. 4, (2022), 2663–2672. https://doi.org/10.1016/j.aej.2021.08.040
20. Jalili, B., Sadighi, S., Jalili, P., and Ganji, D. D. "Characteristics of ferrofluid flow over a stretching sheet with suction and injection." ***Case Studies in Thermal Engineering***, Vol. 14, (2019), 100470. https://doi.org/10.1016/j.csite.2019.100470
21. Brinkman, H. C. "The Viscosity of Concentrated Suspensions and Solutions." ***The Journal of Chemical Physics***, Vol. 20, No. 4, (1952), 571–571. https://doi.org/10.1063/1.1700493
22. Bourantas, G. C., and Loukopoulos, V. C. "MHD natural-convection flow in an inclined square enclosure filled with a micropolar-nanofluid." ***International Journal of Heat and Mass Transfer***, Vol. 79, (2014), 930–944. https://doi.org/10.1016/j.ijheatmasstransfer.2014.08.075
23. Hussanan, A., Ismail, Z., Khan, I., Hussein, A. G., and Shafie, S. "Unsteady boundary layer MHD free convection flow in a porous medium with constant mass diffusion and Newtonian heating." ***The European Physical Journal Plus***, Vol. 129, No. 3, (2014), 46. https://doi.org/10.1140/epjp/i2014-14046-x
24. Khan, U., Ahmed, N., and Mohyud-Din, S. T. "Numerical investigation for three dimensional squeezing flow of nanofluid in a rotating channel with lower stretching wall suspended by carbon nanotubes." ***Applied Thermal Engineering***, Vol. 113, (2017), 1107–1117. https://doi.org/10.1016/j.applthermaleng.2016.11.104
25. Mohyud-Din, S., Khan, U., Ahmed, N., and Hassan, S. "Magnetohydrodynamic Flow and Heat Transfer of Nanofluids in Stretchable Convergent/Divergent Channels." ***Applied Sciences***, Vol. 5, No. 4, (2015), 1639–1664. https://doi.org/10.3390/app5041639
26. Zang, Q., Liu, J., Lu, L., and Lin, G. "A NURBS-based isogeometric boundary element method for analysis of liquid sloshing in axisymmetric tanks with various porous baffles." ***European Journal of Mechanics - B/Fluids***, Vol. 81, (2020), 129–150. https://doi.org/10.1016/j.euromechflu.2020.01.010
27. Hashemi, M. S. "A novel simple algorithm for solving the magneto-hemodynamic flow in a semi-porous channel." ***European Journal of Mechanics - B/Fluids***, Vol. 65, (2017), 359–367. https://doi.org/10.1016/j.euromechflu.2017.05.008
28. Srinivasacharya, D., and Jagadeeshwar, P. "Flow Over an Exponentially Stretching Porous Sheet with Cross-diffusion Effects and Convective Thermal Conditions." ***International Journal of Engineering, Transaction A: Basics***, Vol. 31, No. 1, (2018), 120–127. https://doi.org/10.5829/ije.2018.31.01a.17
29. Sureshkumar, D., and Ethiraj, N. "Experimental and Finite Element Analysis of Single Stage Single Point Incremental Forming." ***International Journal of Engineering, Transaction A: Basics***, Vol. 34, No. 10, (2021), 2259–2265. https://doi.org/10.5829/ije.2021.34.10a.07
30. Bhaskara Rao, J., and Beatrice Seventline, J. "Estimation of Roughness Parameters of A Surface Using Different Image Enhancement Techniques." ***International Journal of Engineering, Transaction B: Applications***, Vol. 30, No. 5, (2017), 652–658. https://doi.org/10.5829/idosi.ije.2017.30.05b.04
31. Fereidoon, A., and Mohammadian, M. "Young s Modulus of Single and Double Walled Carbon Nanocones Using Finite Element Method." ***International Journal of Engineering, Transaction C: Aspects***, Vol. 27, No. 9, (2014), 1467–1474. https://doi.org/10.5829/idosi.ije.2014.27.09c.17
32. Sheel, T. K., and Obi, S. "Acceleration of bluff body calculation using MDGRAPE-2." ***International Journal of Engineering, Transactions A - Basics***, Vol. 23, No. 2, (2010), 169–176. Retrieved from https://www.sid.ir/en/Journal/ViewPaper.aspx?ID=213089

Persian Abstract

چکیده

این مقاله انتقال حرارت و سرعت زاویه‌ای نانوسیال اتیلن گلیکول میکروقطبی را بر روی باله‌های مثلثی، مستطیلی و پخ روی ورق کششی تحلیل می‌کند. نوآوری این مقاله بررسی پارامترهای جریان نانوسیال عبوری از باله‌های مختلف روی سطح کششی است. روش اجزای محدود برای حل معادلات حاکم انتخاب شده است. دمای نانوسیال در فضای باله‌ها گرم و برابر با دمای سطح است. مقدار دما ۳۰ درجه سانتی‌گراد است. حداکثر مقادیر دمای نانوسیال در آخرین باله سطوح وجود دارد. با عبور جریان نانوسیال از اولین باله‌های سطح، دمای جریان از ۲۵ درجه سانتی‌گراد به ۳۱ درجه سانتی‌گراد می‌رسد و در انتهای سطح، دما از ارزش بالایی برخوردار است. حداکثر سرعت زاویه‌ای اتیلن گلیکول در $x=0.9$ برای حالت پخ و مستطیل و حداقل دما در $x=0.8$ برای ۳ باله مختلف رخ می‌دهد. سرعت زاویه‌ای برای نانوسیال در حالت‌های مثلثی و پخ ۶/۵درصد بزرگتر از بافل‌های دیگر است.